IOP Publishing Phys. Med. Biol. 66 (2021) 095009 https://doi.org/10.1088/1361-6560/abef88

Physics in Medicine & Biology

IPEM Institute of Physics and Engineering in Medicine

OPEN ACCESS

RECEIVED
28 January 2021

REVISED
9 March 2021

ACCEPTED FOR PUBLICATION
17 March 2021

PUBLISHED
23 April 2021

PAPER

Physical characterization of ^{3}He ion beams for radiotherapy and comparison with ^{4}He

Felix Horst[1], **Dieter Schardt**[1], **Hiroshi Iwase**[2], **Christoph Schuy**[1], **Marco Durante**[1,3] and **Uli Weber**[1]

[1] GSI Helmholtzzentrum für Schwerionenforschung, Biophysics Department, D-64291 Darmstadt, Germany
[2] KEK, Radiation Science, 1-1 Oho, Tsukuba, Ibaraki, 305-0801, Japan
[3] Technische Universität Darmstadt, Institut für Festkörperphysik, D-64289 Darmstadt, Germany

E-mail: u.weber@gsi.de

Keywords: helium ion therapy, particle therapy, Bragg curve, nuclear fragmentation, heavy ion therapy, Monte Carlo simulation

Supplementary material for this article is available online

Abstract

There is increasing interest in using helium ions for radiotherapy, complementary to protons and carbon ions. A large number of patients were treated with ^{4}He ions in the US heavy ion therapy project and novel ^{4}He ion treatment programs are under preparation, for instance in Germany and Japan. ^{3}He ions have been proposed as an alternative to ^{4}He ions because the acceleration of ^{3}He is technically less difficult than ^{4}He. In particular, beam contaminations have been pointed out as a potential safety issue for ^{4}He ion beams. This motivated a series of experiments with ^{3}He ion beams at Gesellschaft für Schwerionenforschung (GSI), Darmstadt. Measured ^{3}He Bragg curves and fragmentation data in water are presented in this work. Those experimental data are compared with FLUKA Monte Carlo simulations. The physical characteristics of ^{3}He ion beams are compared to those of ^{4}He, for which a large set of data became available in recent years from the preparation work at the Heidelberger Ionenstrahl-Therapiezentrum (HIT). The dose distributions (spread out Bragg peaks, lateral profiles) that can be achieved with ^{3}He ions are found to be competitive to ^{4}He dose distributions. The effect of beam contaminations on ^{4}He depth dose distribution is also addressed. It is concluded that ^{3}He ions can be a viable alternative to ^{4}He, especially for future compact therapy accelerator designs and upgrades of existing ion therapy facilities.

1. Introduction

Proton and carbon ion radiotherapy are nowadays established methods for cancer treatment in several countries. In recent years, also helium ions are back in the interest for clinical cases where neither protons nor carbon ions are ideally suited. Helium ions show intermediate properties between protons and carbon ions with regards to radiation physics (lateral scattering and fragmentation) and radiobiology (Grün *et al* 2015, Krämer *et al* 2016). In the US heavy ion therapy project at the Lawrence Berkeley National Laboratory, 2054 patients were treated with passively scattered ^{4}He ions between 1975 and 1992 (Castro and Quivey 1977, Saunders *et al* 1985, Alonso *et al* 1989, Ludewigt *et al* 1991). Currently, patient treatment with scanned ^{4}He ions at the Heidelberger Ionenstrahl-Therapiezentrum (HIT) in Germany is about to go into operation and will start a new era in particle radiotherapy. At NIRS, Japan, a multi-ion therapy concept including ^{4}He ions is currently set up (Inaniwa *et al* 2017, 2020, Mizushima *et al* 2020) and also other ion therapy facilities, for instance CNAO in Italy and MedAustron in Austria, consider technical upgrades for helium ions (Norbury *et al* 2020).

In the original proposal of the HIT facility (HICAT), which was compiled by a working group at the Gesellschaft für Schwerionenforschung (GSI) in Darmstadt, Germany, the use of the more exotic ^{3}He isotope was foreseen instead of ^{4}He (Bär *et al* 2000, Haberer *et al* 2004). Therefore, a series of experiments with high energy ^{3}He ions was conducted at GSI in 2004 with the aim to explore their potential application in ion beam therapy. Physical and dosimetric as well as radiobiological experiments were performed. However, only few of the results obtained in those experiments can be found in the literature today: one article by Fiedler *et al* (2006) presents PET images of phantoms irradiated with ^{3}He ions and another article by Elsässer *et al* (2010) presents cell survival data. The remaining physics/dosimetry data are unpublished up to now.

The rationale for the proposal of ^{3}He ion therapy in the HICAT proposal was the assumption that it could be technically difficult to accelerate and deliver clean ^{4}He beams using the HIT accelerator design (pre-acceleration in a 5 m long injector linac followed by a 6.5 Tm synchrotron). In the linac, ^{4}He ions can only be accelerated in their fully stripped charge state $^{4}He^{2+}$ because otherwise the final energy would be too low for injection into the synchrotron. Contamination with heavier ions is a known issue for $^{4}He^{2+}$ beams (Winkelmann *et al* 2012, Burigo *et al* 2020, Mizushima *et al* 2020) because they have a charge-to-mass-ratio (q/m) similar to several other fully stripped ions like $^{12}C^{6+}$, $^{14}N^{7+}$, $^{16}O^{8+}$, $^{20}Ne^{10+}$ and $^{36}Ar^{18+}$. Those ion species, if present in the acceleration phase of the synchrotron, can not be magnetically separated from the primary ^{4}He ions anymore and would be accelerated and delivered to the patient together with the therapy beam. At HIT, those technical issues were solved by installing a dedicated helium ion source, operating it with high purity ^{4}He gas (Helium 6.0) and adding a safety system based on a residual gas mass spectrometer that can detect gas leaks immediately (Winkelmann *et al* 2012). Previous clinical data exists only for ^{4}He and their lateral scattering was expected to be superior to ^{3}He due to their higher mass. Therefore, preparation of helium ion therapy at HIT was continued with ^{4}He and is meanwhile in a fully operational status.

Recently, experimental data for ^{4}He ions obtained during the preparation for helium ion therapy at HIT have been reported in several publications (Krämer *et al* 2016, Tessonnier *et al* 2017a, 2017b, 2017c, Horst *et al* 2017, Rovituso *et al* 2017, Horst *et al* 2019). Combined with the ^{3}He data measured at GSI in 2004, this allows now a direct comparison of the physical properties of ^{3}He and ^{4}He ion beams. Therefore, part of the physics/dosimetry data for ^{3}He ions (nuclear fragmentation and Bragg curves in water) obtained at GSI was re-analyzed and is presented in this work together with the available ^{4}He data from HIT. This comparison is supported by simulations using the FLUKA Monte Carlo code. The problem of contaminations in ^{4}He beams and accelerator design aspects are briefly discussed as well.

2. Interaction of ^{3}He and ^{4}He ions with matter

The most important characteristic of ions for radiotherapy is their finite range in matter. An ion penetrating through material slows down continuously while transferring energy to atomic electrons and this electronic energy loss increases the slower the ion becomes. This increase of energy loss with decreasing velocity causes a dose maximum at the end of its range which is known as Bragg peak. For ions with different atomic number Z and mass number A, the range at the same velocity scales with the A/Z^{2}-ratio (Schardt *et al* 2010). Therefore, the velocity (or the energy per nucleon) required to reach the same water depth is larger for ^{3}He than for ^{4}He. For a range of 30 cm in water, considered as the maximum target depth for ion beam radiotherapy, the required energies are 220 MeV/u for ^{4}He and 260 MeV/u for ^{3}He ions, respectively.

An important argument for using helium ions for radiotherapy are their scattering properties. The reduced lateral scattering compared to the lighter protons causes a sharper lateral dose fall-off at large penetration depths (Tessonnier *et al* 2018), therefore, one could expect the same trend for ^{3}He ions and the heavier ^{4}He isotope. However, the lateral deflection of an ion in the Coulomb field of the target nuclei is not only affected by its mass but also by its velocity (Weber and Kraft 2009, Schardt *et al* 2010). Therefore, the increased lateral scattering of ^{3}He ions due to their lower mass is partly compensated by the higher velocity needed to reach the same penetration depth as with ^{4}He ions.

Another important interaction for light and heavy ions is nuclear fragmentation (Schardt *et al* 2010). Even if the difference between the ^{3}He and ^{4}He nucleus is only one neutron, there are remarkable differences between their nuclear fragmentation properties: ^{4}He ions can break up into ^{3}He, ^{3}H, ^{2}H and ^{1}H fragments plus neutrons (Norbury *et al* 2020) while the only possible fragments of ^{3}He ions are ^{2}H and ^{1}H plus neutrons. Since projectile fragments are produced at roughly the same velocity as the primary ions, their ranges scale with A/Z^{2} of the primary ion range. Neutron-deficient fragments of the same element as the primary ion consequently stop before the Bragg peak while practically all other lighter fragments can penetrate beyond the Bragg peak creating the characteristic *fragment tail* in the depth dose profile of light and heavy ions. In the depth dose profile of ^{4}He ions that effect can be observed for its ^{3}He fragments which cause a dose build-up proximal to the Bragg peak. Since ^{2}He nuclei do not exist (two protons alone can not form a bound state), this dose build-up is missing in ^{3}He depth dose profiles where all possible fragments stop after the Bragg peak and contribute to the fragment tail. Secondary neutrons have very long interaction lengths and their effect on the dose profiles can be neglected in a first approximation.

The attenuation of the primary ions along their path through material (or the patient tissue) is determined by the total reaction cross section σ_R. It is the main physical parameter affecting the ratio of Bragg peak dose to entrance dose (peak-to-entrance ratio), therefore a small reaction cross section is a favorable property for ion therapy. The question of whether the reaction cross section of water (H_2O), the reference medium in radiotherapy and fundamental component of biological tissue, is smaller for ^{3}He or ^{4}He ions is not straightforward to answer. On one hand, one could expect that the smaller radius of the ^{3}He nucleus compared to ^{4}He would lead to a smaller reaction cross section (geometrical approximation: $\sigma_R \sim A^{2/3}$ (Bradt and Peters 1950, Durante and Cucinotta 2011)). On the other hand, one could also speculate that the double-magic ^{4}He nucleus might be stabilized by nuclear shell effects leading to a smaller reaction cross section for ^{4}He projectiles. Measurements at 790 MeV/u (Tanihata *et al* 1985) indicate the latter, however, other experiments around 50–100 MeV/u measured almost equal reaction cross sections for both ion species (Millburn *et al* 1954, Ingemarsson *et al* 2000, 2001). A theoretical study by Ingemarsson and Lantz (2003) implies that the ratio of the reaction cross sections for ^{3}He and ^{4}He is energy-dependent due to the different matter density distributions in the two nuclei. The present work allows the first direct comparison of ^{3}He and ^{4}He nuclear reaction cross sections on water targets in the energy range relevant for ion therapy, since recent ^{4}He cross section measurements at HIT (Horst *et al* 2017, 2019) were performed at energies comparable to the ^{3}He experiments carried out at GSI in 2004.

3. Materials and methods

The following section describes the experimental setups for the characterization of ^{3}He ion beams and the Monte Carlo simulations performed in this work.

3.1. Experimental setups

The penetration of high energy ^{3}He ions through water was characterized using two different experimental setups. The experiments were performed in Cave A at GSI where ^{3}He ion beams with energies between 110 and 225 MeV/u were delivered by the SIS18 heavy ion synchrotron.

3.1.1. Scintillator telescope for nuclear fragmentation measurements

The experimental setup to study nuclear fragmentation of 200 MeV/u ^{3}He ions in water consisted of three scintillation detectors. A ^{3}He pencil beam with low intensity ($\sim 10^3$ particles s^{-1}) impinged on a thin start

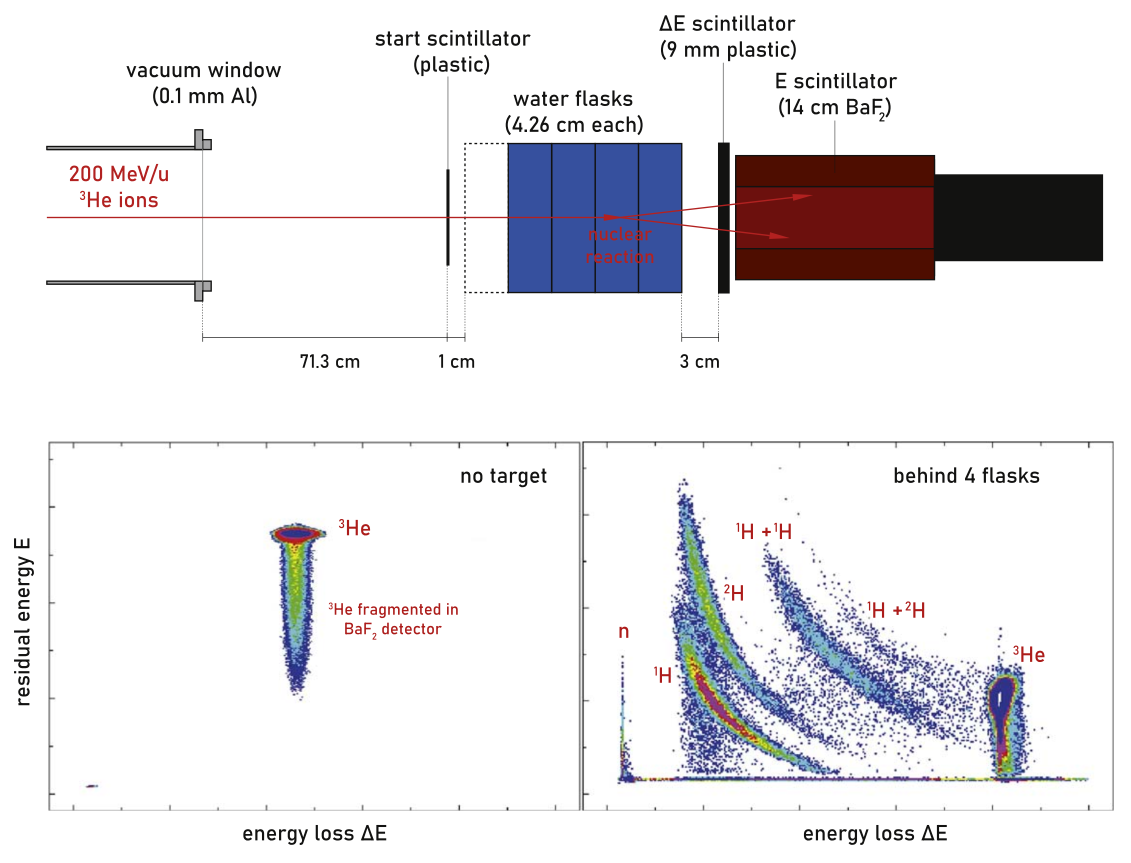

Figure 1. Experimental setup to measure the attenuation of 200 MeV/u ^{3}He ions in water and the build-up of fragments and examples of particle identification spectra.

scintillator and triggered the event-by-event data acquisition (a typical VME data acquisition system, similar to that described by Haettner *et al* (2013)). After the start scintillator, the primary ions penetrated a water absorber of varying thickness (5 flasks with a water-equivalent thickness of 4.26 cm each). The transmitted ^{3}He ions or the produced fragments, respectively, were then stopped in a ΔE-E-telescope consisting of a 9 mm plastic scintillator and a 14 cm thick BaF_2 scintillator. The ΔE-E-spectra provided the particle identification for separation of the different fragment species and the primary ions.

Figure 1 shows a schematic of the experimental setup and two examples of ΔE-E-spectra. All event clusters are well separated. The event numbers recorded for each particle were analyzed by graphical cuts and normalized to the number of trigger events in the start scintillator. Due to the low number of possible fragmentation channels for ^{3}He, the analysis of the multiplicity states (^{1}H + ^{1}H, ^{1}H + ^{2}H) was also straightforward. The uncertainty of the measured attenuation and yields includes different components: the systematic uncertainty of the particle identification was estimated by varying the graphical cuts. The other systematic uncertainties (e.g. non-water materials like the flasks in the beam path and detector thresholds) were estimated as 10%. The statistical uncertainty from the limited number of recorded events were also included in the error bars, but are negligibly small.

The scintillator telescope was placed close to the end of the water target (3 cm distance) to maximize its acceptance (~10° relative to the entrance surface of the thickest target). The BaF_2 scintillator used had a hexagonal shape (inner diameter: 8.5 cm, outer diameter: 10 cm) and the plastic scintillator was slightly larger. For the primary ^{3}He ions it can be assumed that the telescope had full acceptance while not all fragments could be detected, since they can have rather broad angular distributions.

3.1.2. Water column for Bragg curve measurements

For the measurement of ^{3}He Bragg curves in water, a precision water column with two large area parallel plate ionization chambers (IC) (Schardt *et al* 2007) was used. The IC were read out by Keithley K6517A electrometers. The ratio between the charges released in the two IC is a measure of the laterally integrated dose. Between two measurements (~10^8 particles per synchrotron spill) the thickness of the water column was varied. The length of the water column was varied using a stepper motor and read-out by an optical linear encoder (manufactured by Heidenhain) with 1 μm relative accuracy. Figure 2 shows a schematic of the experimental setup.

The water equivalent thickness of the offset materials (vacuum window, IC, quartz windows, air gap) is well known. Each component has been characterized in advance by determining the Bragg curve shift when inserting them into the beam path. The uncertainty of the absolute Bragg peak position measured with the water column is estimated to ~500 μm where the main limiting factor is the calibration at the lowest thickness. The relative distances of the Bragg peaks at different energies are more accurate and have an estimated uncertainty of ~50 μm.

As seen in figure 2, the measurement ionization chamber (IC2) was fixed at 8 cm distance from the end of the water column. This distance has to be taken into account for comparison of the experimental Bragg curves with calculations because even if most of the primary ions are collected by the IC2, a significant fraction of fragments emitted at large angles can scatter out of its acceptance (up to about 30% depending on the water thickness and energy). Details of the IC2 were described by Pfuhl *et al* (2018).

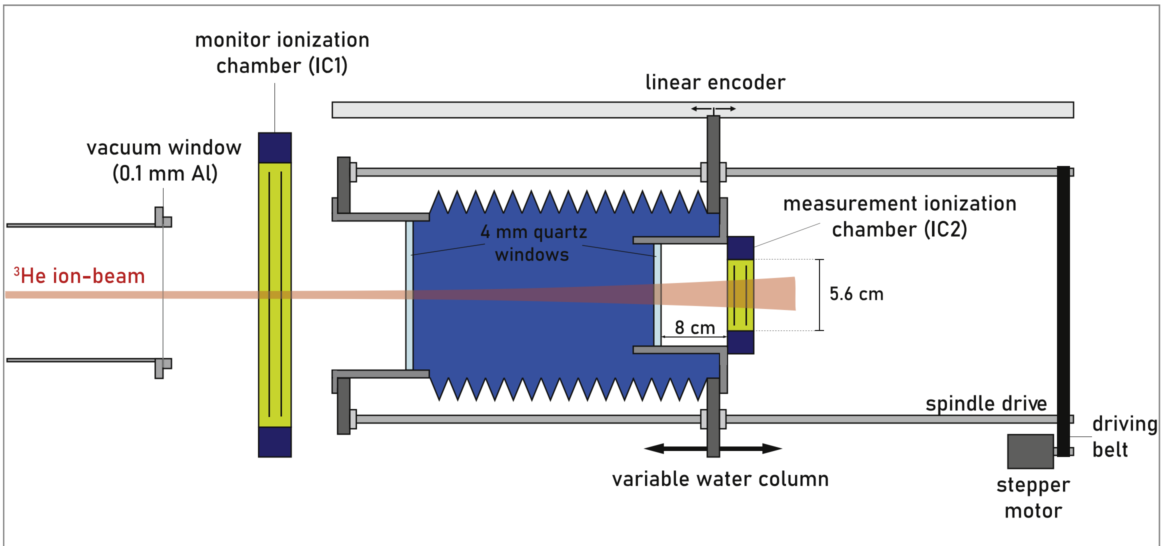

Figure 2. Experimental setup to measure ^{3}He Bragg curves in water.

3.2. Monte Carlo simulations

Monte Carlo simulations were performed with the FLUKA code (version 2020.0.3) (Ferrari *et al* 2005, Böhlen *et al* 2014, Battistoni *et al* 2015, 2016). The FLUKA nuclear reaction models for ^{4}He ions have been optimized (Aricò *et al* 2019) and the improved models are implemented in the FLUKA version 2020.0.3 used in this work.

The two experiments described in section 3.1 were reproduced by simulations. The targets were approximated as consisting entirely of water, neglecting the plastic walls of the flasks in the fragmentation experiment and the quartz windows of the water column in the Bragg curve experiment but using their water equivalent thicknesses. The scintillator telescope in the fragmentation setup was modeled as a cylindrical slab with a diameter of 9 cm where the incoming particle fluences were scored. The IC in the Bragg curve setup were modeled as 1 cm thick air-filled volumes, the IC1 as a block with lateral dimensions of 20 $\times$ 20 cm and the IC2 as a cylinder with a diameter of 5.6 cm. The distances from the end of the water targets to the detectors (see figures 1 and 2) were taken into account. Therefore, the simulations had to be performed step by step, i.e. one simulation per water depth.

For additional simulations of laterally integrated depth dose profiles, lateral dose profiles, fluence distributions and LET profiles, a simple slab geometry consisting of a 50 cm long water cylinder with 20 cm diameter was used and the entire profiles were scored in single simulations. For re-simulation of a ^{4}He Bragg curve with beam contaminations, where the reference data was measured at Brookhaven National Laboratory using a different approach (extended field and a small detector (La Tessa *et al* 2016)) with limited acceptance, the diameter of the scoring radius was varied until a best match between measurement and simulation was observed. Furthermore, the measurement was in polyethylene instead of water, and therefore converted into water-equivalent thickness.

The initial energy spread was assumed to have a full width at half maximum of 0.1%, which is a realistic assumption for ion beams from a synchrotron. For simulation of spread out Bragg peaks (SOBPs), the inital energy spread of the single energy layers was increased to 1% to mimic a ripple filter. This results in broader Bragg peaks and makes it easier to cover the SOBP with a homogeneous dose (Weber and Kraft 1999).

The mean ionization potential of water was set to 78 eV for all simulations in accordance with the recommendations in the recent ICRU 90 report (Seltzer 2016).

Dose and fluence were scored with the USRBIN card. LET spectra were scored with the USRYIELD card. From the LET spectra, the dose averaged LET was calculated offline.

4. Results and discussion

In the following section the experimental results for nuclear fragmentation and Bragg curves together with FLUKA simulations are presented. With the FLUKA simulation models validated against the measured Bragg curves, the comparison of ^{3}He and ^{4}He ions can be extended to SOBPs representing a more realistic radiotherapy scenario. Finally, also the aspect of contaminations in ^{4}He beams and parameters relevant for accelerator design are discussed.

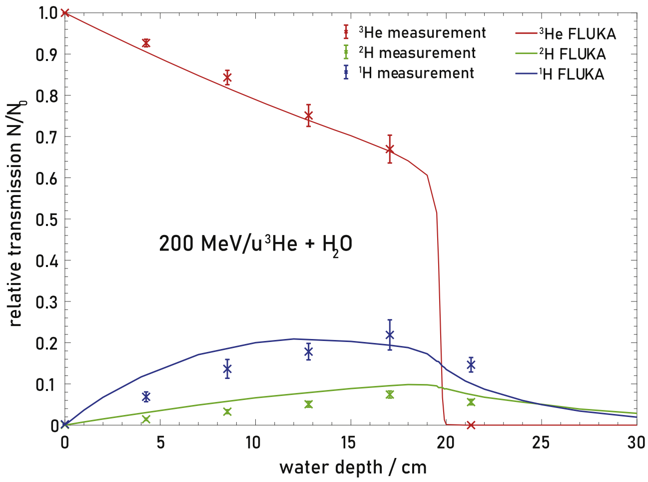

Figure 3. Attenuation of primary ^{3}He ions and build-up of ^{2}H and ^{1}H fragments for 200 MeV/u ^{3}He ions in water. The symbols show the experimental data and the lines show the FLUKA predictions.

4.1. Nuclear fragmentation

Figure 3 shows the experimental data for fragmentation of 200 MeV/u ^{3}He ions in water together with FLUKA simulations.

With increasing thickness of the water target the number of primary ^{3}He ions decreases while deuteron (^{2}H) and proton (^{1}H) fragments build up. Behind the primary ion range (~19.5 cm) only fragments can be detected. This trend is reasonably well reproduced by the FLUKA simulations as shown in figure 3. Concerning the attenuation of the primary ^{3}He ions, the FLUKA prediction (red line) slightly over-estimates the attenuation behind the two thinner targets but agrees again with the measurements behind thick targets within their uncertainties.

Fitting of the attenuation at 4.26 and 8.52 cm (residual energy of 173 and 143 MeV/u) with an exponential function yields a charge-changing cross section, which for ^{3}He ions is practically equal to the total reaction cross section, of 600 ± 70 mb. This is significantly lower compared to the cross section of 800 ± 58 mb measured for 220 MeV/u ^{4}He ions on water targets (Horst *et al* 2019). Measurements at 200 and 220 MeV/u are comparable since the energy dependence of nuclear reaction cross sections is very flat in this energy region. ^{3}He turns out to be the more stable helium nucleus in the therapeutic energy range, which makes it particularly interesting for ion beam therapy.

4.2. Bragg curves

Figure 4 shows the measured Bragg curves for 110, 170, 190 and 225 MeV/u ^{3}He ions compared the FLUKA predictions.

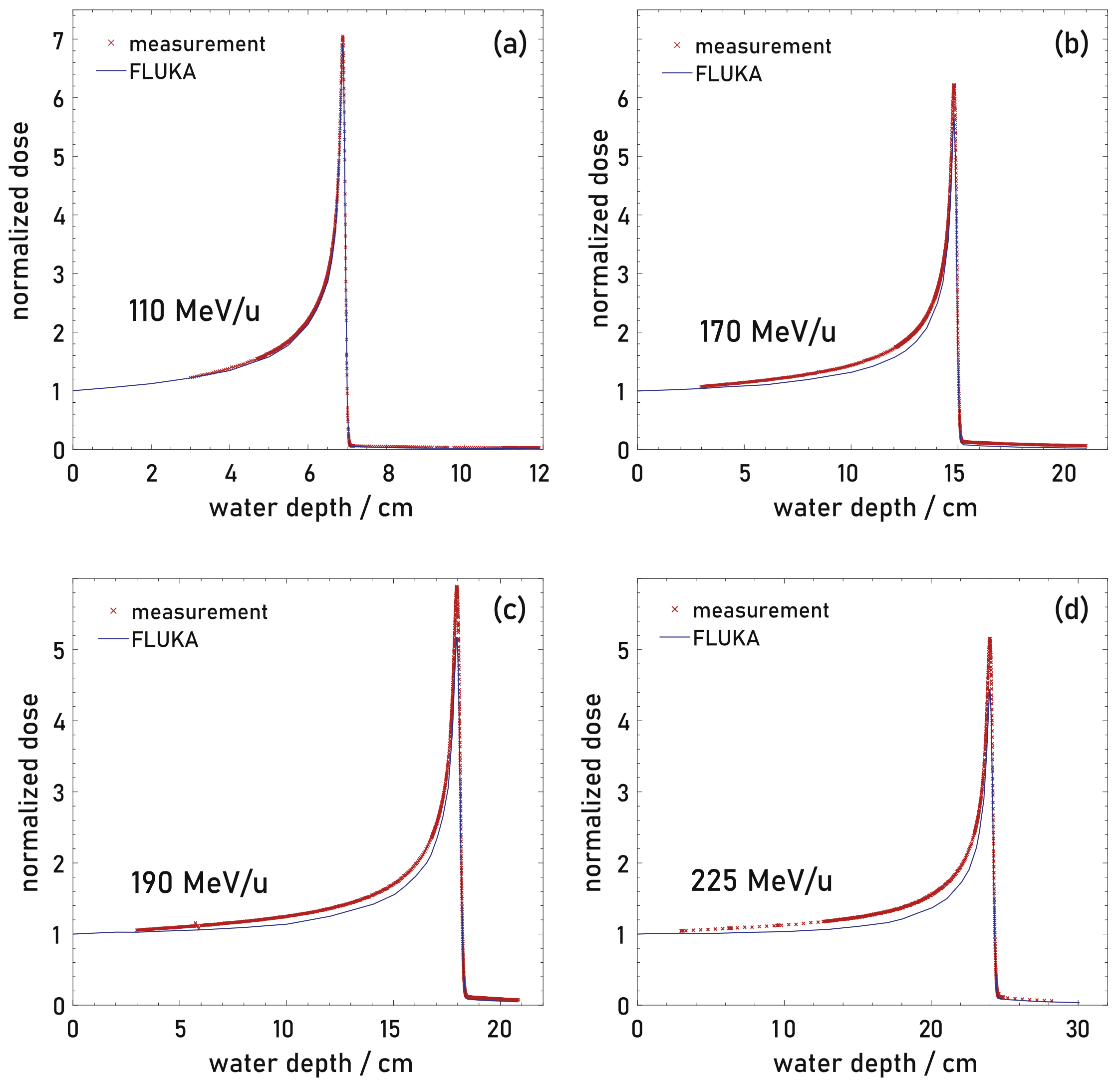

Figure 4. Bragg curves for 110, 170, 190 and 225 MeV/u ^{3}He ions in water normalized to the entrance. The red symbols show the experimental data and the lines show the FLUKA predictions. The measured Bragg curves were extrapolated to zero water depth for the normalization.

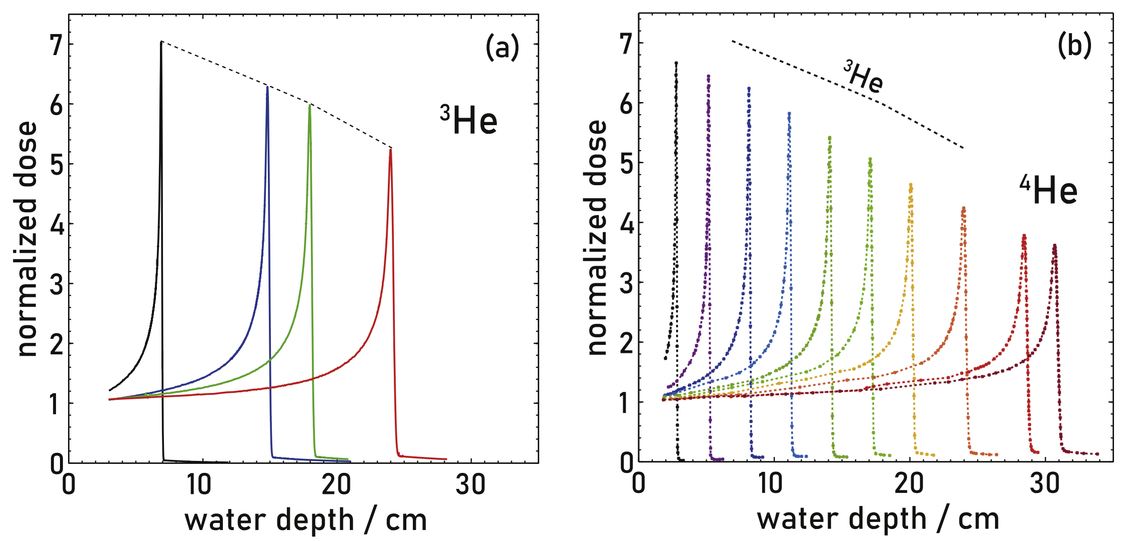

Figure 5. Measured ^{3}He (panel (a)) and ^{4}He Bragg curves (panel (b)) normalized to the entrance. The Bragg curves were extrapolated to zero water depth for the normalization. The Bragg curves for ^{3}He ions were measured at GSI (this work) and those for ^{4}He ions at HIT (published by Tessonnier *et al* (2017c)). The dashed line indicates the ^{3}He peaks in both panels for better comparison.

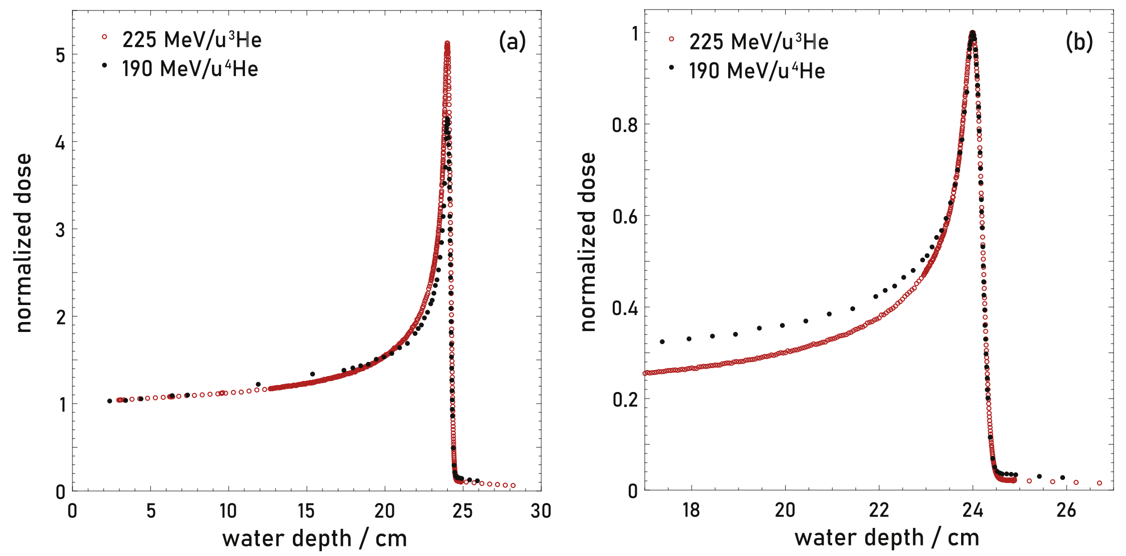

Figure 6. Comparison of measured ^{3}He and ^{4}He Bragg curves with the same range. Bragg curve for 225 MeV/u ^{3}He (red open symbols) was measured at GSI (this work) and that for 190 MeV/u ^{4}He (black filled symbols) at HIT (published by Tessonnier *et al* (2017c)). Panel (a) shows the two Bragg curves normalized to the entrance and panel (b) shows a zoom at the same curves normalized to the peak value.

The FLUKA results and the measured Bragg curves are normalized to the entrance. The experimental Bragg curves had to be extrapolated for this normalization since a measurement at zero target thickness could not be performed due to the fixed windows of the water column.

The absolute Bragg peak positions were well reproduced by the FLUKA simulations with deviations from the experimental data between 0.1 mm (110 MeV/u) and 0.7 mm (225 MeV/u), corresponding to relative differences between 0.1 and 0.4%.

While for the lowest energy (panel (a)) the shape of the measured Bragg curve is reproduced with good accuracy by the FLUKA simulation, some disagreements can be observed for the higher energies. The peak-to-entrance ratio obtained in the measurements is underestimated by the FLUKA simulations and the difference increases towards higher energies. The discrepancy is only marginal for the 110 MeV/u Bragg curve (about 1.5%) but increases to 10% for 170 MeV/u, 16% for 190 MeV/u and 18% for 225 MeV/u. A possible explanation for these deviations could be inaccuracies in the total reaction cross section models, similar to what has been found for ^{4}He ions in previous studies (Aricò *et al* 2019). In that specific case, finetuning of the physics model parameters within the FLUKA code against experimental cross section data led to an improved dose calculation accuracy.

For the three higher energies (panels (b)–(d)), the dose behind the Bragg peak (fragment tail) is slightly underestimated by the FLUKA simulations. As visible in figure 3, the secondary proton yield behind the primary ion range was slightly underestimated as well which could be one explanation. Furthermore, the IC2 signal is also quite sensitive to the angular distribution of the fragments which is more complicated for Monte Carlo codes to predict than the total yields.

Since the available experimental data for nuclear reactions induced by ^{3}He ions is rather limited, deviations between Monte Carlo simulations and measurements of that magnitude are not particularly surprising and the overall agreement can be considered reasonable. In future studies, the ^{3}He Bragg curves and fragmentation data provided in this work could serve as reference to validate and optimize radiation transport codes for ^{3}He ions in the therapeutic energy range.

Figure 5 shows the measured ^{3}He Bragg curves compared with corresponding ^{4}He data. The experimental data for ^{4}He measured at HIT, Heidelberg, were reported by Tessonnier *et al* (2017c) and the data points were taken from their publication. From the comparison of the two ion species it can be observed, that the peak-to-entrance ratio of ^{3}He ions at the same range is larger than that of ^{4}He ions (see dashed line in panel (b)). This can possibly be explained by the lower nuclear reaction cross section of ^{3}He compared to ^{4}He projectiles as discussed in section 4.1. Since for ^{3}He less primary ions fragment before reaching the end of their range due to the lower reaction cross section (see section 4.1), this translates into a higher Bragg peak.

Figure 6 shows the two Bragg curve measurements with the closest range (225 MeV/u ^{3}He and 190 MeV/u ^{4}He) in comparison. The depth values of the ^{4}He Bragg curve were compressed by 0.3% to precisely match the ranges. The larger peak-to-entrance ratio for ^{3}He is clearly visible in panel (a) and the zoom in panel (b) demonstrates that the peak width and the distal edge are identical for both measurements. Therefore, the lower peak-to-plateau ratio observed for ^{4}He ions can not be caused by differences in the energy spread at the GSI and HIT accelerators and beamlines. Also the different acceptance of the two experimental setups can not be a reason, since the PTW PeakFinder used for the ^{4}He measurements (Tessonnier *et al* 2017c) has even a larger acceptance than the water column used for the ^{3}He measurements (8.16 cm diameter of the ICs instead of 5.6 cm, see figure 2).

4.3. Spread out Bragg peaks

After assessing the differences between ^{3}He and ^{4}He ions in the pristine Bragg curves, the question comes up if the higher peak-to-entrance ratio observed for ^{3}He translates into advantages for the irradiation of extended volumes. Therefore, as a more clinically relevant scenario, the irradiation of SOBPs into a water phantom was simulated using the FLUKA Monte Carlo code. For those simulations, a set of Bragg curves with fine energy steps, corresponding to range steps of $\sim$1 mm, was pre-calculated for both ^{3}He and ^{4}He ions to optimize their weights to irradiate an SOBP. Figure 7 shows a comparison between ^{3}He and ^{4}He SOBPs of different extensions (1, 2 and 5 cm). The SOBPs are centered around 14.5 cm which is a realistic target depth for average tumors.

An advantage in the dose distribution of ^{3}He ions proximal to the SOBP can be observed for all three examples. However, the difference between ^{3}He and ^{4}He becomes larger for smaller SOBPs. The dose in the fragment tail is slightly larger for the ^{3}He SOBPs compared to ^{4}He. Those differences can be understood by considering their different fragmentation characteristics: one one hand, ^{3}He ions have less probability to fragment (see section 4.1) and therefore produce higher Bragg peaks (see figure 4) compared to ^{4}He. On the other hand, all possible fragments of ^{3}He (^{2}H and ^{1}H) have on average longer ranges than the primary ions

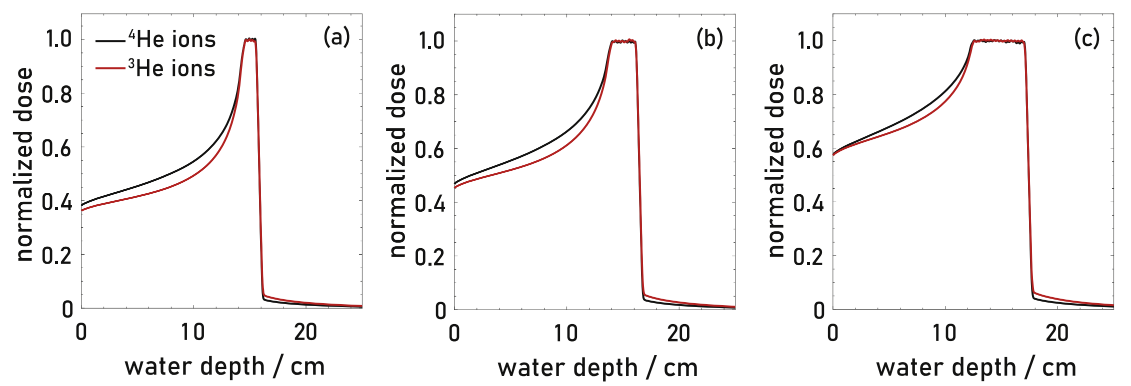

Figure 7. ^{3}He and ^{4}He SOBPs with extensions of 1 cm (panel (a)), 2 cm (panel (b)) and 5 cm (panel (c)) calculated using the FLUKA Monte Carlo code. Absorbed dose without RBE-weighting is shown.

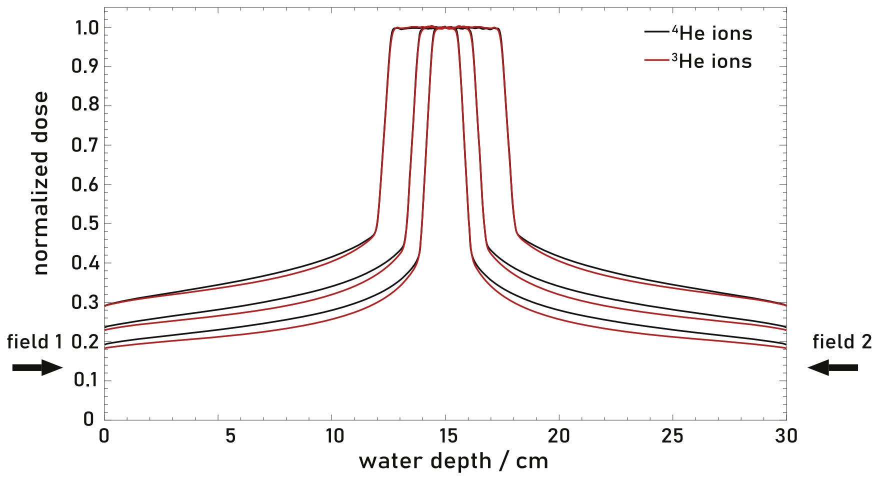

Figure 8. ^{3}He and ^{4}He SOBPs for two opposing fields with extensions of 1, 2 and 5 cm calculated using the FLUKA Monte Carlo code. Absorbed dose without RBE-weighting is shown.

according to the A/Z^2 scaling (see section 2), while for primary ^{4}He ions some of the fragments have a shorter (^{3}He) or the same (^{1}H) range. As a result, the ^{3}He depth dose profiles have less dose contributions before the Bragg peak, but a higher dose in the fragment tail than the ^{4}He profiles.

In clinical practice, tumors are normally not irradiated with only one field but using multiple fields from different directions. To understand if the lower dose proximal to the Bragg peak would cancel out with the higher dose in the fragment tail, irradiations with two opposing fields were mimicked as well, shown in figure 8.

The same trend as in figure 7 can be observed. Also for opposing fields, the use of ^{3} He instead of ^{4}He ions would allow a lower dose in the healthy tissue at the same dose to the target volume. The maximum differences in the studied examples are around 10% for the 1 cm SOBP. A reduction of the dose to the normal tissue of that order could be relevant for organs at risk with a steep dose-response relationship like for instance the spinal cord (Karger *et al* 2006).

It should be noted that the FLUKA calculated Bragg curve for 170 MeV/u ^{3}He ions has a 10% lower peak-to-entrance ratio than what was found in the measurement (see panel (c) of figure 4). Therefore, the actual differences of SOBPs irradiated with ^{3}He and ^{4}He can be expected to be even more pronounced than what is visible in the simulation results shown in figures 7 and 8.

4.4. Lateral dose profiles

The reduced lateral scattering of helium ions compared with protons is one of the main reasons for considering them for radiotherapy (Grün *et al* 2015, Krämer *et al* 2016). Therefore, this point was also investigated in detail for ^{3}He and ^{4}He ions by simple analytical approximations and detailed Monte Carlo simulations.

The lateral deflections by multiple Coulomb scattering can be approximated by a Gaussian distribution (Highland 1975). If the material and thickness are kept constant and relativistic effects are neglected, the influence of the atomic number Z and mass number A and the velocity v of the projectile on the lateral beam spread σ_θ after traversing a thin target can be described by equation (1) (Weber and Kraft 2009)

$$\sigma_\theta \sim \frac{Z}{A \cdot v^2}. \quad (1)$$

Because the scattering happens in the Coulomb field of the target nuclei, a higher charge of the projectile increases the lateral beam spread. On the other hand, increasing the projectile mass or velocity has an inverse effect because a higher forward momentum makes the beam become more rigid.

In table 1, the ratio between the lateral beam spread σ_θ of ^{3}He and ^{4}He ions with same ranges in water calculated according to equation (1) are reported. A rather constant ratio of 1.16–1.18 is observed for the given energies. For comparison: the corresponding ratio of σ_θ for protons and ^{12}C ions lies between 3.3 and 3.4.

The SCATTMAN transport code (Weber 1996, Schardt *et al* 2010) was used to study the beam broadening due to lateral scattering based on the Highland approximation (Highland 1975). Figure 9 shows calculated beam envelopes of ^{3}He and ^{4}He pencil beams in a typical ion therapy setup at the energies listed in table 1.

The ion beams exit the vacuum tube through a thin double window consisting of two pairs of 100 μm hostaphan foil with supporting 100 μm kevlar tissue layers. Then they penetrate through the beam monitoring system, typically consisting of two multi wire proportional chambers and three parallel plate IC. Even if the

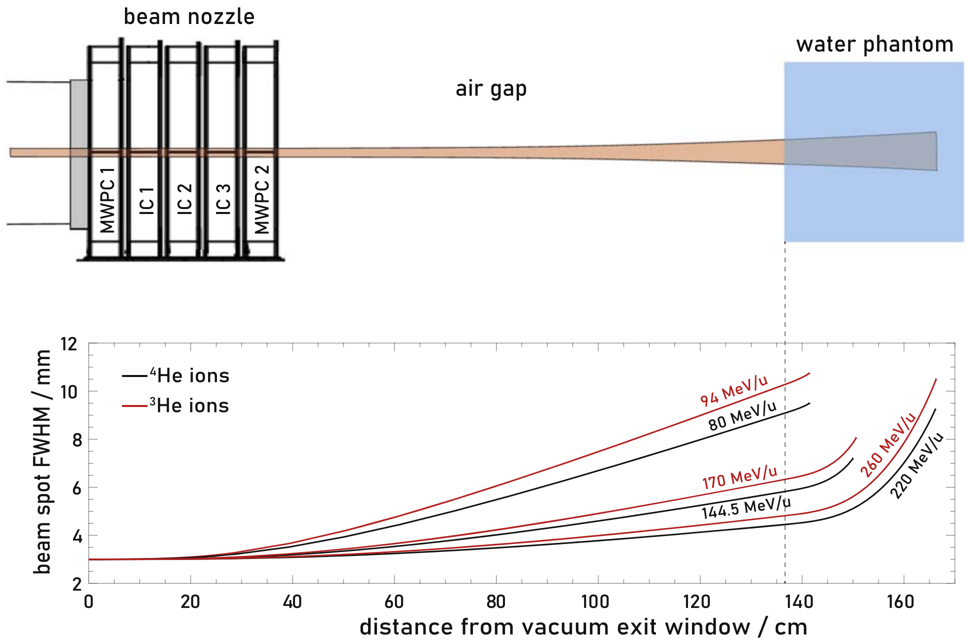

Figure 9. Broadening of ^{3}He and ^{4}He pencil beams calculated using the SCATTMAN multiple scattering transport code (Weber 1996, Schardt *et al* 2010). An inital focus of 3 mm was assumed. The simulation setup mimics the HIT treatment rooms.

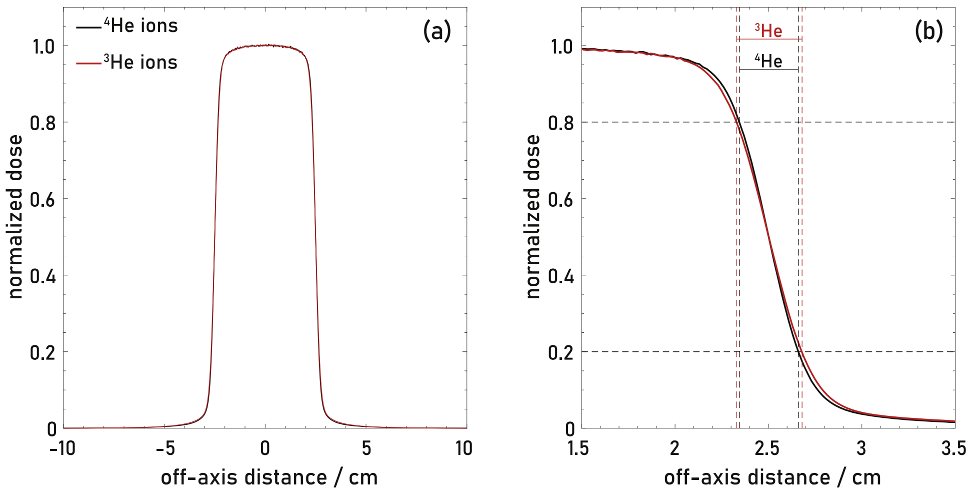

Figure 10. Lateral dose profiles for ^{3}He and ^{4}He ions in the center of a 5 cm SOBP (at a depth of 15 cm) calculated using the FLUKA Monte Carlo code. Panel (a) shows the full profile and panel (b) shows a zoom at the lateral falloff.

Table 1. Ratio of lateral beam spread for ^{3}He and ^{4}He ions with the same range in water.

Range in water	5 cm	15 cm	30 cm
^{3}He energy	94 MeV/u	170 MeV/u	260 MeV/u
^{3}He velocity	12.54 cm ns^{-1}	16.00 cm ns^{-1}	18.70 cm ns^{-1}
^{4}He energy	80 MeV/u	144.5 MeV/u	220 MeV/u
^{4}He velocity	11.69 cm ns^{-1}	15.01 cm ns^{-1}	17.62 cm ns^{-1}
^{3}He/^{4}He σ_θ ratio	1.16	1.17	1.18

water equivalent thickness of these components sums up to only 1.7 mm, their effect on the angular beam spread is significant. After passing the beam monitor system, the ions pass along a 1 m air gap and when hitting the water phantom the beams are already considerably widened up. Finally, the ions are slowed down in the water phantom and the lateral spread grows further until they reach the end of their range. For high energies the

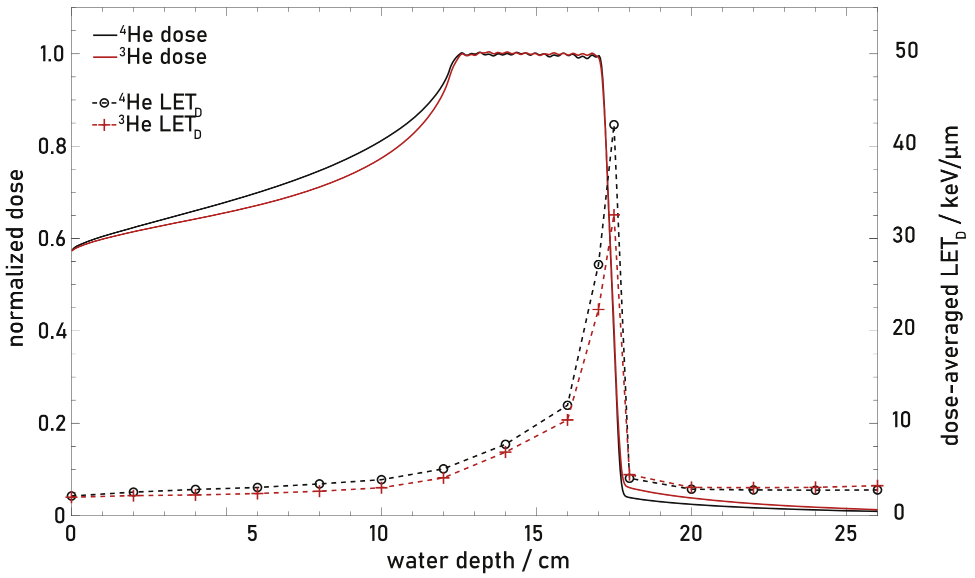

Figure 11. ^{3}He and ^{4}He absorbed dose and LET$_D$ profiles for a 5 cm SOBP calculated with the FLUKA Monte Carlo code.

lateral scattering in the water phantom is the dominant contributor to the final beam size while for low energies the scattering in the beam monitor system is more relevant.

The beam envelopes are slightly larger for ^{3}He than for ^{4}He ions due to their lower mass. However, the difference is not very pronounced (factor 1.16–1.18 as discussed above).

To understand if the differences in lateral scattering between ^{3}He and ^{4}He within the water phantom or patient are relevant, additional FLUKA simulations have been performed. Figure 10 shows ^{3}He and ^{4}He lateral dose profiles in the center of a $5 \times 5 \times 5$ cm^3 dose cube (at a depth of 15 cm of the 5 cm SOBP shown in figures 7 and 11). In panel (a) of figure 10 the ^{3}He and ^{4}He profiles can hardly be distinguished. Only in the zoom at the lateral falloff (panel (b)), the slightly stronger broadening of the ^{3}He profile can be noticed. The lateral penumbra can be characterized by the $d_{80,20}$ distance (Safai *et al* 2008). It is about 16% larger for ^{3}He ($d_{80,20} = 0.36$ cm) than for ^{4}He ($d_{80,20} = 0.31$ cm), which is comparable with the factor 1.16–1.18 estimated from equation (1). For target volume extensions in the order of centimeters, those differences in the lateral profile of the two ion species are practically negligible. The reason for the small differences observed in the lateral profiles of ^{3}He and ^{4}He ions are the different energies per nucleon required to reach the same depth (see section 2).

4.5. Radiobiological aspects

All comparisons above focused on absorbed dose profiles, however, in ion beam therapy, absorbed dose weighted by the relative biological effectiveness (RBE) is the quantity of interest. For real tumor irradiations, a flat biological SOBP is optimized using a suitable biophysical model. Therefore, the question how comparable the radiobiology of ^{3}He and ^{4}He ions is should also be adressed.

The RBE effects of helium ions are moderate compared to carbon ions, however, they are more pronounced than for protons and the depth-dependence of the RBE should be considered in treatment planning (Grün *et al* 2015). From the Berkeley trial a clinical RBE of 1.2–1.3 for ^{4}He SOBPs was reported by Castro and Quivey (1977) while RBE values measured in the entrance channel are close to 1 (Phillips *et al* 1977, Mairani *et al* 2016).

At the same LET, no differences in the radiobiology of ^{3}He and ^{4}He ions are to be expected. However, the energy per nucleon to reach the same depth is larger for ^{3}He than for ^{4}He ions (in the order of 20%) which causes a slightly reduced LET for ^{3}He at the same (residual) range. In a mixed radiation field, the dose-averaged linear energy transfer LET$_D$ can serve as a rough indicator of the radiation quality (Grün *et al* 2019). Figure 11 shows the LET$_D$ profiles for ^{3}He and ^{4}He ions for the 5 cm SOBP shown in panel (b) of figure 7.

The LET$_D$ profiles for ^{3}He and ^{4}He ions are comparable but not fully identical. In the shown example the LET$_D$ ranges from $\sim$2 keV μm^{-1} at the entrance up to $\sim$30–40 keV μm^{-1} at the distal falloff of the SOBP. For ^{3}He ions, it is lower by 6%–23% compared with ^{4}He due to their different energies per nucleon at a given depth. The less dense ionization tracks of ^{3}He ions could result in a slight reduction of the biological effectiveness in the SOBP compared to ^{4}He. For some cases, this might compensate part of the advantages observed for ^{3}He in the peak-to-entrance ratio of physically optimized SOBPs (figures 7 and 11).

The interplay between physical and biological properties of different ion species is very complex and besides the radiation quality it depends also on the combination of the radiosensitivity (low LET α/β-ratios) of normal and tumor tissue and on the dose per fraction (Grün *et al* 2015). A detailed radiobiological comparison of the two ion species is out of scope of the present study but future investigations into that topic could either be based on the local effect model (LEM IV) or the modified microdosimetric model (mMKM) which both have been shown to be accurate for helium ions (Elsässer *et al* 2010, Mairani *et al* 2017, Mein *et al* 2019). A computational study on the RBE of ^{3}He ions based on Monte Carlo simulations and a parametrized RBE model has been performed by Taleei *et al* (2016).

For verification of radiobiological models and calculations, a variety of cell survival data for ^{3}He and ^{4}He ions can be found in the PIDE database (Friedrich *et al* 2012). For example, Furusawa *et al* (2000) reported ^{3}He survival curves for different cell lines measured at several energies.

4.6. Contaminations in ^{4}He beams

When ^{4}He ion beams are used for radiotherapy, the contamination with heavier ions can be a serious issue. Panel (a) of figure 12 shows a Bragg curve of a contaminated 236 MeV/u ^{4}He beam measured at the NASA Space Radiation Laboratory (NSRL) (La Tessa *et al* 2016, Burigo *et al* 2020) of Brookhaven National Laboratory (BNL), USA (the same Bragg curve was also shown by Durante and Paganetti (2016)).

The measured Bragg curve (symbols) with small extra Bragg peaks at about 1/3 of the primary ion range can reasonably be reproduced by FLUKA simulations (lines). To fit the measured curve, the contamination with 236 MeV/u ^{12}C, ^{14}N and ^{16}O ions of 0.15%, 0.25% and 0.20% was assumed. This estimate of the contamination level is in the same order like measurements by Burigo *et al* (2020). The most probable origin of those ions is residual air in the ion source (Beebe *et al* 2015, Burigo *et al* 2020). The NSRL beamline is mostly used for radiobiological irradiations, for which a slightly contaminated beam might still be acceptable. However, when patients are treated with ^{4}He ions such beam contaminations must be avoided since the Bragg peaks of the heavier ions would irradiate the healthy tissue. Winkelmann *et al* (2012) describe a safety system to detect gas leaks in the ion source implemented at HIT and Mizushima *et al* (2020) describe a prototype of a beam diagnostic device under development at NIRS to monitor the purity of ^{4}He beams in their medical beamlines.

Panel (b) if figure 12 shows a 150 MeV/u ^{4}He Bragg curve calculated with different contamination levels (0.01%, 0.1% and 0.5% of ^{12}C, ^{14}N and ^{16}O ions). From this comparison, it gets clear that the contamination of ^{4}He therapy beams should be kept below 0.01%, which is also the limit that Winkelmann *et al* (2012) have pointed out.

There are ideas to exploit that effect for online imaging and range verification during radiotherapy, by intentionally contaminating a ^{12}C ion beam with ^{4}He ions (Graeff *et al* 2018, Mazzucconi *et al* 2018, Volz *et al* 2020). The patient is then treated with ^{12}C ions while the ^{4}He ions with a three times higher range are detected after exiting the patient.

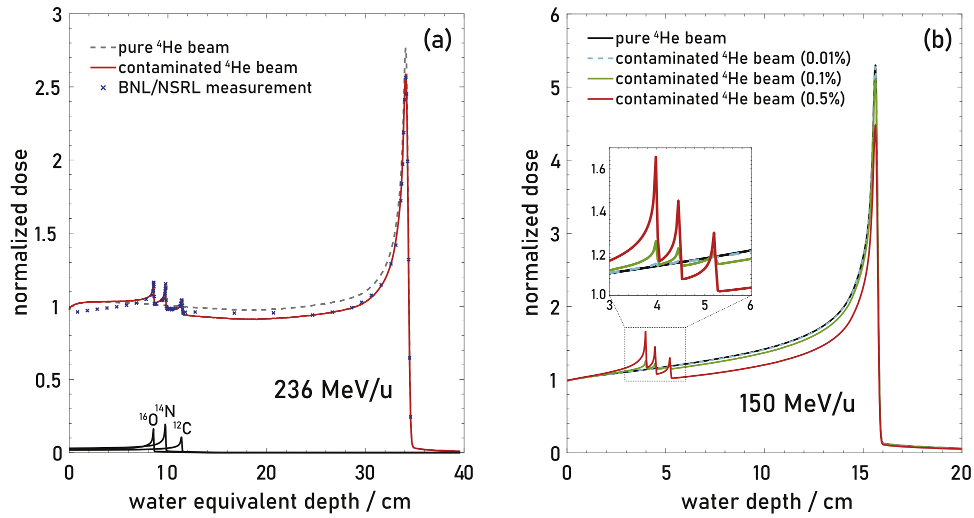

Figure 12. A 236 MeV/u ^{4}He Bragg curve with beam contaminations measured at the NSRL beamline at Brookhaven National Laboratory (courtesy of Chiara La Tessa, Trento University; also shown by Durante and Paganetti (2016)) together with FLUKA simulations (panel (a)) and a calculated 150 MeV/u ^{4}He Bragg curve with different contamination levels (panel (b)).

Table 2. Accelerator design aspects for ^{3}He and ^{4}He therapy machines. The given parameters are for a range of 30 cm in water.

Parameter	^{3}He	^{4}He
Kinetic energy per nucleon	260 MeV/u	220 MeV/u
Total kinetic energy	780 MeV	880 MeV
Velocity	0.624 c	0.588 c
Magnetic rigidity	3.74 Tm	4.52 Tm
q/m (partly stripped, fully stripped)	1/3, 2/3	1/4, 1/2

4.7. Accelerator design aspects

The design of new accelerators for ion beam therapy is an active field of research (Owen *et al* 2016, Farr *et al* 2018). The overall footprint of the accelerator determines to a large extent the total costs of an ion beam therapy facility. As also pointed out by Taleei *et al* (2016), ^{3}He ions could be very attractive for compact therapy accelerator designs. Table 2 compares parameters of ^{3}He and ^{4}He that are relevant for design and construction of accelerators.

As already mentioned in section 2, the kinetic energy per nucleon (i.e. the velocity β) required to reach a depth of 30 cm (the typical design goal of therapy accelerators) is higher for ^{3}He than for ^{4}He. However, the total kinetic energy and the magnetic rigidity is considerable lower for ^{3}He. There are no commercial cyclotron designs for carbon ion therapy available up to now. The company IBA is currently developing a 400 MeV/u machine called C-400 (Jongen *et al* 2010) comparable to what was proposed in the EULIMA project (Mandrillon *et al* 1987). For ^{3}He ions, compact and cost-effective cyclotron designs may be feasible due to the relatively low final velocity (relativistic effects that complicate the acceleration in cyclotrons are still moderate at 260 MeV/u) and the less rigid beams would allow lighter magnets in the cyclotron, beam transport lines and gantry with a lower energy consumption.

Contamination levels below 0.01% are a reasonable design goal for therapy accelerators. As discussed in section 4.6 the acceleration of clean ^{3}He ion beams is easier than for ^{4}He due to the more unique q/m-ratios of 1/3 or 2/3. In the HICAT study (Bär *et al* 2000), the acceleration of $^{3}He^{1+}$ ions ($q/m = 1/3$) in the linac injector was proposed because typical electron cyclotron resonance (ECR) ion sources can yield higher intensities for this charge state than for $^{3}He^{2+}$ ($q/m = 2/3$). After the stripper foil behind the linac, possible $^{12}C^{4+}$ contaminations are removed before injection into the synchrotron. The typical injection linacs in compact therapy synchrotrons are too short to reach the injection energy for $^{4}He^{1+}$ and for $^{4}He^{2+}$, contaminations with $q/m = 1/2$ (e.g. $^{12}C^{6+}$, $^{14}N^{7+}$, $^{16}O^{8+}$, $^{20}Ne^{10+}$ or $^{36}Ar^{18+}$) can not be removed easily because they are already fully stripped.

At synchrotron-based ion therapy facilities, a single ion source could be operated together for ^{3}He ions ($^{3}He^{1+}$) and protons (H_3^{1+}) if a few minutes of switching time between the two species is acceptable (Bär *et al* 2000) while for ^{4}He a dedicated ion source is preferable to avoid the above mentioned beam contaminations and a safety system to monitor the beam purity should be installed (Winkelmann *et al* 2012, Mizushima *et al* 2020). Therefore, if existing ion therapy facilities should be upgraded to helium ions, ^{3}He could be a cost-saving alternative or an option for facilities where no space for a further ion source is available.

^{3}He is known to be very expensive and its prize can fluctuate strongly (Shea and Morgan 2010). This aspect has to be considered when thinking about routine ion therapy operation with ^{3}He beams because the ion source needs to be supplied with gas. Therefore, a rough estimate of the additional operating cost due to ^{3}He supply is presented in the following: the gas consumption of an ECR ion source lies in the order of a few cm^{-3}/h. Assuming a ^{3}He gas prize of 3000 Euro per liter at atmospheric pressure and a gas consumption of 10 cm^{-3}/h one obtains a conservative estimate of the additional operating costs of 30 Euro/h. This can be a non-negligible cost factor, but is still low compared with the regular operating costs of an ion therapy facility.

5. Conclusion and outlook

The re-introduction of radiotherapy with ^{4}He ions currently ongoing at different facilities could stimulate the interest in helium ion therapy worldwide.

Besides ^{4}He ions, also radiotherapy with ^{3}He ions was proposed in the past, mainly to avoid the potential problem of beam contaminations. In this article, experimental fragmentation data and Bragg curves in water for ^{3}He ions in the therapeutical energy range measured at GSI, Darmstadt, are presented. The measured ^{3}He Bragg curves could be reproduced reasonably well by FLUKA Monte Carlo simulations with slight deviations towards higher energies. On basis of the experimental data supported by Monte Carlo simulations, the physical characteristics of ^{3}He and ^{4}He ions were compared in detail. This comparison showed that ^{3}He ions exhibit more interesting features for radiotherapy than only the possibility of producing clean helium beams. The physical depth dose profiles of ^{3}He turned out to be competitive to those of ^{4}He. In the studied examples, the peak-to-entrance ratio of physically optimized ^{3}He SOBPs was slightly better than that achievable with ^{4}He ions. This can be mainly associated to the lower primary ion attenuation due to the smaller nuclear reaction cross section of ^{3}He compared to ^{4}He. The sparing effect for ^{3}He increases as the extension of the SOBP decreases. The fragment tail in ^{3}He depth dose profiles is slightly more pronounced than for ^{4}He due to their different fragmentation channels.

The beam broadening due to lateral scattering is stronger for ^{3}He compared to ^{4}He, however, the differences are only marginal. Lateral dose profiles in the SOBP were found to be almost similar for both ions. This is because the initial energy per nucleon required to reach the same depth is higher for ^{3}He than for ^{4}He and the higher velocity of ^{3}He partly compensates for their 25% lower mass.

^{3}He ions have a lower LET compared to ^{4}He ions with the same range, therefore, slight differences in their RBE can be expected. These radiobiological aspects should be addressed in future comparative studies supported by a appropriate biophysical model (e.g. mMKM or LEM IV).

The present study shows that ^{3}He ions could be an interesting alternative to ^{4}He as they can produce comparable dose profiles, even with some advantages. Especially for future compact therapy accelerator designs, ^{3}He ions seem attractive since they would require considerably smaller magnets due to their lower magnetic rigidity than ^{4}He. If ^{4}He ions are used for radiotherapy, a dedicated ion source and a monitoring system which can ensure the beam purity (contaminations with heavier ions below 0.01%) should be installed. For ^{3}He ion beams a separate ion source and an additional safety system would not be necessary because they are basically free from contaminations due to their unique q/m-ratio. Therefore the upgrade of existing synchrotron-based ion therapy facilities to ^{3}He might be easier and less expensive than to ^{4}He.

To compare ^{3}He and ^{4}He ions for real radiotherapy scenarios, a treatment planning study including a suitable RBE model would be useful. The experimental data for ^{3}He ions presented in this work can be used to validate the basic data used as input for treatment planning systems.

Acknowledgments

We want to thank Jakob Naumann from the Heidelberg Ion Beam Therapy Center who participated in the measurement of the ^{3}He Bragg curves at GSI, provided us with helpful information about the technical implementation of ^{4}He ions at HIT and gave us useful comments to the present study. We also thank Klaus Tinschert from the ion source department at GSI for helpful explanations about the operation and gas consumption of ECR ion sources and the differences in acceleration of ^{3}He and ^{4}He. Chiara La Tessa from the University of Trento is acknowledged for providing the ^{4}He Bragg curve measured at the NASA Space Radiation Laboratory.

ORCID iDs

Marco Durante https://orcid.org/0000-0002-4615-553X

References

Alonso J R, Bercovitz J, Chu W T, Ludewigt B, Nyman M, Singh R, Stradtner C, Tafelski R and Walton R 1989 Relocation of the helium ion radiotherapy program from the 184″ synchrocyclotron to the BEVALAC *Proc. 1989 IEEE Particle Accelerator Conf.* 1, pp 669–71 (https://ieeexplore.ieee.org/document/73217)

Aricò G, Ferrari A, Horst F, Mairani A, Reidel C-A, Schuy C and Weber U 2019 Developments of the nuclear reaction and fragmentation models in FLUKA for ion collisions at therapeutic energies *Proc. 15th Int. Conf. on Nuclear Reaction Mechanisms (Varenna, Italy)* pp 321–6 (http://cds.cern.ch/record/2669357)

Bär R, Dolinskii A, Eickhoff H, Haberer T, Peters A, Rau M, Schlitt B and Spiller P 2000 HICAT—the Heavy Ion Cancer Therapy accelerator facility for the clinic in Heidelberg *Technical Description*

Battistoni G *et al* 2015 Overview of the FLUKA code *Ann. Nucl. Energy* **82** 10–8

Battistoni G *et al* 2016 The FLUKA Code: an accurate simulation tool for particle therapy *Frontiers Oncol.* **6** 116

Beebe E, Alessi J, Binello S, Kanesue T, McCafferty D, Morris J, Okamura M, Pikin A, Ritter J and Schoepfer R 2015 Reliable operation of the Brookhaven EBIS for highly charged ion production for RHIC and NSRL *AIP Conf. Proc.* **1640** 5–11

Böhlen T, Cerutti F, Chin M, Fassò A, Ferrari A, Ortega P, Mairani A, Sala P, Smirnov G and Vlachoudis V 2014 The FLUKA Code: developments and challenges for high energy and medical applications *Nucl. Data Sheets* **120** 211–4

Bradt H L and Peters B 1950 The heavy nuclei of the primary cosmic radiation *Phys. Rev.* **77** 54–70

Burigo L, Gehrke T, Jäkel O, Sivertz M, Olsen T, Rusek A, Obcemea C and Greilich S 2020 Beam characterization at NSRL for radiobiological experiments–phase 1 *J. Instrum.* **15** T10004–10004

Castro J R and Quivey J M 1977 Clinical experience and expectations with helium and heavy ion irradiation *Int. J. Radiat. Oncol.*Biol.*Phys.* **3** 127–31 Particles and Radiation Therapy Second International Conference

Durante M and Cucinotta F A 2011 Physical basis of radiation protection in space travel *Rev. Mod. Phys.* **83** 1245

Durante M and Paganetti H 2016 Nuclear physics in particle therapy: a review *Rep. Prog. Phys.* **79** 096702
Elsässer T *et al* 2010 Quantification of the relative biological effectiveness for ion beam radiotherapy: Direct experimental comparison of proton and carbon ion beams and a novel approach for treatment planning *Int. J. Radiat. Oncol.**Biol.**Phys.* **78** 1177–83
Farr J B, Flanz J B, Gerbershagen A and Moyers M F 2018 New horizons in particle therapy systems *Med. Phys.* **45** e953–83
Ferrari A, Sala P R, Fassò A and Ranft J 2005 *FLUKA: A Multi-Particle Transport Code CERN-2005-10* (https://cds.cern.ch/record/898301)
Fiedler F, Crespo P, Parodi K, Sellesk M and Enghardt W 2006 The feasibility of in-beam PET for therapeutic beams of ^{3}He *IEEE Trans. Nucl. Sci.* **53** 2252–9
Friedrich T, Scholz U, Elsässer T, Durante M and Scholz M 2012 Systematic analysis of RBE and related quantities using a database of cell survival experiments with ion beam irradiation *J. Radiat. Res.* **54** 494–514
Furusawa Y, Fukutsu K, Aoki M, Itsukaichi H, Eguchi-Kasai K, Ohara H, Yatagai F, Kanai T and Ando K 2000 Inactivation of aerobic and hypoxic cells from three different cell lines by accelerated ^{3}He-, 12C- and ^{20}Ne-Ion Beams *Radiat. Res.* **154** 485–96
Graeff C, Weber U, Schuy C, Saito N, Volz L, Piersimoni P, Seco J and Kraemer M 2018 [OA027] Helium as a range probe in carbon ion therapy *Phys. Med.* **52** 11
Grün R, Friedrich T, Krämer M, Zink K, Durante M, Engenhart-Cabillic R and Scholz M 2015 Assessment of potential advantages of relevant ions for particle therapy: a model based study *Med. Phys.* **42** 1037–47
Grün R, Friedrich T, Traneus E and Scholz M 2019 Is the dose-averaged let a reliable predictor for the relative biological effectiveness? *Med. Phys.* **46** 1064–74
Haberer T, Debus J, Eickhoff H, Jäkel O, Schulz-Ertner D and Weber U 2004 The Heidelberg Ion Therapy Center *Radiother. Oncol.* **73** 186–90
Haettner E, Iwase H, Krämer M, Kraft G and Schardt D 2013 Experimental study of nuclear fragmentation of 200 and 400 MeV/u ^{12}c ions in water for applications in particle therapy *Phys. Med. Biol.* **58** 8265–79
Highland V L 1975 Some practical remarks on multiple scattering *Nucl. Instrum. Methods* **129** 497–9
Horst F, Schuy C, Weber U, Brinkmann K-T and Zink K 2017 Measurement of charge- and mass-changing cross sections for ^{4}He.^{12}C collisions in the energy range 80–220 MeV/u for applications in ion beam therapy *Phys. Rev.* C **96** 024624
Horst F *et al* 2019 Measurement of ^{4}He charge- and mass-changing cross sections on H, C, O, and Si targets in the energy range 70–220 MeV/u for radiation transport calculations in ion-beam therapy *Phys. Rev.* C **99** 014603
Inaniwa T, Kanematsu N, Noda K and Kamada T 2017 Treatment planning of intensity modulated composite particle therapy with dose and linear energy transfer optimization *Phys. Med. Biol.* **62** 5180–97
Inaniwa T, Suzuki M, Lee S H, Mizushima K, Iwata Y, Kanematsu N and Shirai T 2020 Experimental validation of stochastic microdosimetric kinetic model for multi-ion therapy treatment planning with helium-, carbon-, oxygen-, and neon-ion beams *Phys. Med. Biol.* **65** 045005
Ingemarsson A and Lantz M 2003 Geometrical aspects of reaction cross sections for ^{3}He, ^{4}He, and ^{12}C projectiles *Phys. Rev.* C **67** 064605
Ingemarsson A *et al* 2000 New results for reaction cross sections of intermediate energy α-particles on targets from ^{9}Be to ^{208}Pb *Nucl. Phys.* A **676** 3–31
Ingemarsson A *et al* 2001 Reaction cross sections of intermediate energy ^{3}He-particles on targets from ^{9}Be to ^{208}Pb *Nucl. Phys.* A **696** 3–30
Jongen Y *et al* 2010 Compact superconducting cyclotron C400 for hadron therapy *Nucl. Instrum. Methods Phys. Res.* A **624** 47–53
Karger C, Peschke P, Sanchez-Brandelik R, Scholz M and Debus J 2006 Radiation tolerance of the rat spinal cord after 6 and 18 fractions of photons and carbon ions: experimental results and clinical implications *Int. J. Radiat. Oncol.**Biol.**Phys.* **66** 1488–97
Krämer M *et al* 2016 Helium ions for radiotherapy? Physical and biological verifications of a novel treatment modality *Med. Phys.* **43** 1995–2004
La Tessa C, Sivertz M, Chiang I-H, Lowenstein D and Rusek A 2016 Overview of the nasa space radiation laboratory *Life Sci. Space Res.* **11** 18–23
Ludewigt B A, Chu W T, Phillips M H and Renner T R 1991 Accelerated helium-ion beams for radiotherapy and stereotactic radiosurgery *Med. Phys.* **18** 36–42
Mairani A, Magro G, Tessonnier T, Böhlen T T, Molinelli S, Ferrari A, Parodi K, Debus J and Haberer T 2017 Optimizing the modified microdosimetric kinetic model input parameters for proton and ^{4}He ion beam therapy application *Phys. Med. Biol.* **62** N244–56
Mairani A *et al* 2016 Biologically optimized helium ion plans: calculation approach and its in vitro validation *Phys. Med. Biol.* **61** 4283–99
Mandrillon P, Ostojic R, Susini A, Jongen Y, Meulders J P and Ryckewaert G 1987 The EULIMA project *11th Int. Conf. on Cyclotrons and their Applications* p F05
Mazzucconi D, Agosteo S, Ferrarini M, Fontana L, Lante V, Pullia M and Savazzi S 2018 Mixed particle beam for simultaneous treatment and online range verification in carbon ion therapy: proof-of-concept study *Med. Phys.* **45** 5234–43
Mein S *et al* 2019 Biophysical modeling and experimental validation of relative biological effectiveness (RBE) for ^{4}He ion beam therapy *Radiat. Oncol.* **14** 123
Millburn G P, Birnbaum W, Crandall W E and Schecter L 1954 Nuclear radii from inelastic cross-section measurements *Phys. Rev.* **95** 1268–78
Mizushima K, Iwata Y, Muramatsu M, Lee S H and Shirai T 2020 Experimental study on monitoring system of clinical beam purity in multiple-ion beam operation for heavy-ion radiotherapy *Rev. Sci. Instrum.* **91** 023309
Norbury J W *et al* 2020 Are further cross section measurements necessary for space radiation protection or ion therapy applications? Helium projectiles *Frontiers Phys.* **8** 1–30
Owen H, Lomax A and Jolly S 2016 Current and future accelerator technologies for charged particle therapy *Nucl. Instrum. Methods Phys. Res.* A **809** 96–104 Advances in detectors and applications for medicine
Pfuhl T, Horst F, Schuy C and Weber U 2018 Dose build-up effects induced by delta electrons and target fragments in proton bragg curves–measurements and simulations *Phys. Med. Biol.* **63** 175002
Phillips T L, Fu K K and Curtis S B 1977 Tumor biology of helium and heavy ions *Int. J. Radiat. Oncol.**Biol.**Phys.* **3** 109–13 Particles and Radiation Therapy Second International Conference
Rovituso M *et al* 2017 Fragmentation of 120 and 200 MeV u−1 ^{4}He ions in water and PMMA targets *Phys. Med. Biol.* **62** 1310–26
Safai S, Bortfeld T and Engelsman M 2008 Comparison between the lateral penumbra of a collimated double-scattered beam and uncollimated scanning beam in proton radiotherapy *Phys. Med. Biol.* **53** 1729–50
Saunders W *et al* 1985 Helium-ion radiation therapy at the Lawrence Berkeley Laboratory: recent results of a Northern California Oncology Group clinical trial *Radiat. Res.* **104** 227–34
Schardt D, Elsässer T and Schulz-Ertner D 2010 Heavy-ion tumor therapy: physical and radiobiological benefits *Rev. Mod. Phys.* **82** 383–425
Schardt D, Steidl P, Krämer M, Weber U, Parodi K and Brons S 2007 Precision Bragg-curve measurements for light-ion beams in water', GSI Scientific Report *GSI Scientific Report* 2007 p 373

Seltzer S M 2016 ICRU Report 90: key data for ionizing-radiation dosimetry: measurement standards and applications *J. ICRU* **14**

Shea D and Morgan D 2010 The helium-3 shortage: supply, demand, and options for congress *CRS Report for Congress R41419* (https://digital.library.unt.edu/ark:/67531/metadc31373)

Taleei R, Guan F, Peeler C, Bronk L, Patel D, Mirkovic D, Grosshans D R, Mohan R and Titt U 2016 Monte Carlo simulations of ^{3}He ion physical characteristics in a water phantom and evaluation of radiobiological effectiveness *Med. Phys.* **43** 761–76

Tanihata I *et al* 1985 Measurements of interaction cross sections and radii of he isotopes *Phys. Lett.* B **160** 380–4

Tessonnier T, Mairani A, Chen W, Sala P, Cerutti F, Ferrari A, Haberer T, Debus J and Parodi K 2018 Proton and helium ion radiotherapy for meningioma tumors: a Monte Carlo-based treatment planning comparison *Radiat. Oncol.* **13** 2

Tessonnier T *et al* 2017a Dosimetric verification in water of a monte carlo treatment planning tool for proton, helium, carbon and oxygen ion beams at the heidelberg ion beam therapy center *Phys. Med. Biol.* **62** 6579–94

Tessonnier T *et al* 2017b Experimental dosimetric comparison of ^{1}H, ^{4}He, ^{12}C and ^{16}O scanned ion beams *Phys. Med. Biol.* **62** 3958–82

Tessonnier T *et al* 2017c Helium ions at the heidelberg ion beam therapy center: comparisons between FLUKA monte carlo code predictions and dosimetric measurements *Phys. Med. Biol.* **62** 6784–803

Volz L *et al* 2020 Experimental exploration of a mixed helium/carbon beam for online treatment monitoring in carbon ion beam therapy *Phys. Med. Biol.* **65** 055002

Weber U 1996 Volumenkonforme Bestrahlung mit Kohlenstoff-Ionen zur Vorbereitung einer Strahlentherapie *PhD Thesis* Universität Kassel

Weber U and Kraft G 1999 Design and construction of a ripple filter for a smoothed depth dose distribution in conformal particle therapy *Phys. Med. Biol.* **44** 2765–75

Weber U and Kraft G 2009 Comparison of carbon ions versus protons *Cancer J.* **15** 325–32

Winkelmann T, Cee R, Haberer T, Naas B and Peters A 2012 Test bench to commission a third ion source beam line and a newly designed extraction system *Rev. Sci. Instrum.* **83** 02B904